FEASIBILITY OF A PLANET'S HORIZON FOR CAMERA CALIBRATION

Kalani R. Danas Rivera[1*] and Mason A. Peck[1]; [1]Cornell University, Ithaca, NY 14850, [*]krd76@cornell.edu

Abstract. *This work provides a method for intrinsic camera calibration from a single conic correspondence when the image is an ellipse. Given that images of planetary bodies resemble ellipses, the proposed method is attractive for onboard spacecraft camera calibration. This work explores the feasibility of the proposed method when applied to a planet's horizon.*

Introduction. Onboard spacecraft cameras are an immense sensing asset for onboard optical navigation (OPNAV). OPNAV methods enable spacecraft to fulfill their stringent navigation requirements and all rely on a calibrated camera for successful integration. For the case of spacecraft implementing OPNAV near an ellipsoidal planetary body, this paper considers using the image of the planet itself to calibrate the spacecraft camera's intrinsic parameters.

It is well understood that the imaged conic A follows the equality

$$sK^TAK = B \tag{1}$$

where $A, B, K \in \mathbb{R}^{3\times3}$ and s is an unknown scale coefficient. K denotes the intrinsic camera calibration matrix, and B is the reference conic. When B is the apparent conic of an ellipsoid, the following equation gives B as

$$B = Srr^TS - (r^TSr - 1)S \tag{2}$$

where S is the ellipsoid's shape matrix and r is the observer's relative position, respectively.[1] Information from the spacecraft's current state and SPICE kernels inform B. The task of camera calibration seeks a solution for K given known A and B in Eq. (1). Prior works recognize Eq. (1) is non-linear with respect to K and require at least two imaged A for a solution.[2–4] To our knowledge, this work provides the first closed-form solution for K from a single conic. The requirement of a single conic correspondence enables camera calibration from the image of a single planet.

Derivation. This section provides a brief derivation of the proposed camera calibration algorithm. We find it convenient first to partition K into sub-blocks

$$K \triangleq \begin{bmatrix} K_{11} & K_{12} \\ 0_{1\times2} & 1 \end{bmatrix} \tag{3}$$

where

$$K_{11} \triangleq \begin{bmatrix} d_x & \gamma \\ 0 & d_y \end{bmatrix} \quad \text{and} \quad K_{12} \triangleq \begin{bmatrix} u_p \\ v_p \end{bmatrix}. \tag{4}$$

Similarly, we'll also block partitions A and B as follows

$$A \triangleq \begin{bmatrix} A_{11} & A_{12} \\ A_{12}^T & A_{22} \end{bmatrix}, \quad B \triangleq \begin{bmatrix} B_{11} & B_{12} \\ B_{12}^T & B_{22} \end{bmatrix} \tag{5}$$

where $A_{11}, B_{11} \in \mathbb{R}^{2\times2}$, $A_{12}, B_{12} \in \mathbb{R}^{2\times1}$, and $A_{22}, B_{22} \in \mathbb{R}^{1\times1}$. Substituting the block-partitioned matrices reduces Eq. (1) to the system of equations

$$\begin{aligned} sK_{11}^TA_{11}K_{11} &= B_{11} \\ sK_{11}^T(A_{11}K_{12} + A_{12}) &= B_{12} \\ s(K_{12}^TA_{11} + A_{12}^T)K_{11} &= B_{12}^T \\ sK_{12}^T(A_{11}K_{12} + 2A_{12}) + sA_{22} &= B_{22} \end{aligned}. \tag{6}$$

We'll draw attention to the following sub-block equality

$$sK_{11}^TA_{11}K_{11} = B_{11} \tag{7}$$

and apply the $det(\bullet)$ operator to give

$$s^2det(K_{11})^2det(A_{11}) = det(B_{11}) \tag{8}$$

Interestingly, due to K's upper triangular structure

$$det(K) = det(K_{11})det(1) = det(K_{11}). \tag{9}$$

This property of K enables us to solve for s directly. First, applying the $det(\bullet)$ to Eq. (1) gives

$$det(sK^TAK) = s^3det(K_{11})^2det(A) = det(B) \tag{10}$$

from which dividing it by Eq. (8) and re-arranging gives the exact expression

$$s = \frac{det(B)det(A_{11})}{det(A)det(B_{11})} \tag{11}$$

in terms of known A and B. With s known, we can return to Eq. (8). It is well known that for ellipses, $det(A_{11}) > 0$. Applying the $sign(\bullet)$ to Eq. (8) gives

$$sign(s^2det(K_{11})^2det(A_{11})) = sign(det(B_{11})) \tag{12}$$

which reduces to

$$sign(det(B_{11})) = sign(det(A_{11})) > 0. \tag{13}$$

Considering $A_{11}, B_{11} \in \mathbb{R}^{2\times2}$, A_{11} and B_{11} have strictly positive or strictly negative eigenvalues. To ensure A_{11} and B_{11} are strictly positive-definite, we modify A and B to

$$\begin{aligned} A &= \alpha A \\ B &= \beta B \end{aligned} \tag{14}$$

where $\alpha = sign(trace(A_{11}))$ and $\beta = sign(trace(B_{11}))$. With this modification, sA_{11} and B_{11} are symmetric positive definite which enables Cholesky decompositions

$$\begin{aligned} B_{11} &= L_BL_B^T = R_B^TR_B \\ sA_{11} &= L_AL_A^T = R_A^TR_A \end{aligned} \tag{15}$$

where $L_\bullet$ and $R_\bullet$ are lower and upper triangular matrices, respectively. Substituting L_A and L_B produces

$$K_{11}^T L_A L_A^T K_{11} = L_B L_B^T \tag{16}$$

which we can then equate

$$L_A^T K_{11} = L_B^T \tag{17}$$

and solve

$$K_{11} = L_A^{-T} L_B^T = R_A^{-1} R_B \tag{18}$$

in exact terms. With K_{11} known, we move on to the following sub-block equality

$$s K_{11}^T (A_{11} K_{12} + A_{12}) = B_{12} \tag{19}$$

and re-arrange to

$$K_{12} = A_{11}^{-1} \left((s K_{11}^T)^{-1} B_{12} - A_{12} \right) \tag{20}$$

and solve for K_{12}. All pieces of information of unknown K are now known.

Simulation Results. We simulate planetary bodies of varying ellipsoid shapes and pointing geometries to assess our method's camera calibration performance. Table 1 details the semi-axes values used to model each ellipsoid in terms of the planet's polar radius R_p. We examine

Table 1. Ellipsoid Semi-axes

Ellipsoid-Type	a (R_p)	b (R_p)	c (R_p)
Sphere	1.0	1.0	1.0
Oblate	1.5	1.5	1.0
Triaxial	3.0	2.0	1.0

the method's sensitivity to ellipse-fit error by perturbing the semi-major/minor axes and center coordinates of the imaged ellipse A with Gaussian noise $\sim \mathcal{N}(0, \sigma^2)$. Here the proportionality relationship

$$A \propto K^{-T} B K^{-1} \tag{21}$$

gives the imaged ellipse A in pixel coordinates,[1] similar to what an observer would compute. The Gaussian noise perturbation models the effects of edge localization error typical of off-the-shelf edge detection algorithms. After perturbation, we compare the estimated intrinsic parameters with the ground truth and obtain the residual.

The simulation performs a sweep of σ values and obtains the root-sum-square (RSS) of 1000 Monte Carlo runs for each value of σ. To generalize the findings, we divide the RSS value by the ground-truth value to obtain the normalized root-sum-square (NRSS). Figure 1 reports the NRSS of focal lengths and pixel centers for varying ellipsoid shapes under the nadir and off-nadir pointing geometries. In this simulation, the off-nadir pointing geometry places the planet center at a right ascension and declination angles of 2.86° from the camera boresight.

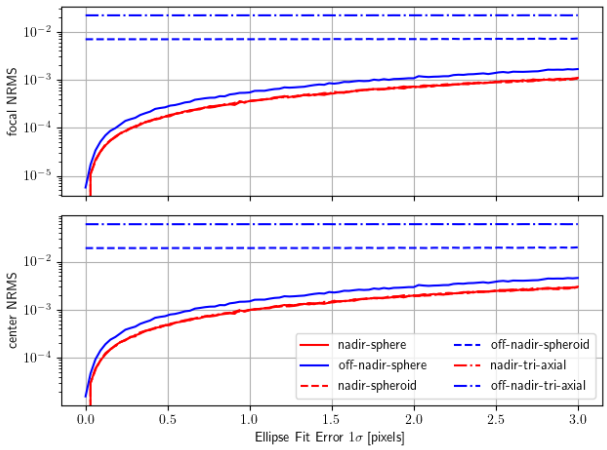

Figure 1. Intrinsic Calibration for Varying Pointing and Varying Ellipsoids

From Fig.1, the proposed method estimates the focal lengths with greater precision than the center coordinates. Since K_{12} is computed from K_{11}, the estimation error of K_{11} propagates to the center coordinate estimates. However, both follow similar trends where nadir-pointing conditions for all ellipsoids provide identical estimates, and off-nadir pointing conditions differ. We are encouraged to see that off-nadir pointing conditions result in NRSS values essentially independent of ellipse fit error for spheroids and triaxial ellipsoids for the simulated σ values. This independence provides constant bounds on our camera calibration method for the general case of off-nadir pointing.

Conclusion. This work provides a novel camera calibration method requiring only one conic correspondence. The one conic requirement enables in-orbit calibration based on imaging the nearest ellipsoidal planet. For spacecraft in Earth orbit, the target may be the Earth or the moon. Future work will implement our method on real images of planetary bodies and discuss the method's resulting performance. We anticipate using images of Saturnian moons as captured by Cassini's narrow-angle camera for our analysis.

References.

[1] J. A. Christian, "A tutorial on horizon-based optical navigation and attitude determination with space imaging systems," *IEEE Access*, vol. 9, pp. 19819–19853, 2021. doi: 10.1109/ACCESS.2021.3051914.

[2] C. Yang, F. Sun, and Z. Hu, "Planar conic based camera calibration," in *Proceedings 15th International Conference on Pattern Recognition. ICPR-2000*, vol. 1, pp. 555–558, IEEE, 2000. doi: 10.1109/ICPR.2000.905398.

[3] H. Huang, H. Zhang, and Y.-m. Cheung, "The common self-polar triangle of concentric circles and its application to camera calibration," in *Proceedings of the IEEE Conference on Computer Vision and Pattern Recognition*, pp. 4065–4072, 2015. doi: 10.1109/CVPR.2015.7299033.

[4] J. Sun, X. Chen, Z. Gong, Z. Liu, and Y. Zhao, "Accurate camera calibration with distortion models using sphere images," *Optics & Laser Technology*, vol. 65, pp. 83–87, 2015. doi: 10.1016/j.optlastec.2014.07.009.